MODELING FLUID FLOW IN HETEROGENEOUS AND ANISOTROPIC POROUS MEDIA

by

Xiaomin Zhao and M. Nafi Toksöz

Earth Resources Laboratory
Department of Earth, Atmospheric, and Planetary Sciences
Massachusetts Institute of Technology
Cambridge, MA 02139

ABSTRACT

Permeability distribution in reservoirs is very important for the flow of water or oil and gas. In this study, the effects of various heterogeneous permeability distributions on the flow field are simulated using the finite difference technique. We have simulated the flow for two types of heterogeneous distributions, one is Gaussian and the other is self-similar or fractal, the latter being much rougher than the former. The results show that the flow is not sensitive to the roughness of the distribution. In the case of lineated heterogeneities, anisotropy in the flow properties occurs. The anisotropy is not very significant if the lineated highly permeable regions are surrounded by less permeable regions. However, in the case of lineated fractures, where the background permeability is small, the flow is very sensitive to the direction of the lineation, such anisotropy can produce orders of magnitude difference in permeability. Furthermore, it is shown that the degree of anisotropy depends on the connectivity of the fractures. The anisotropy decreases with decreasing connectivity.

INTRODUCTION

The transport properties of fluids in reservoirs are controlled by the permeability of the medium. Due to the complexity of geological structures, the distribution of the permeability is usually heterogeneous. The situation becomes more complicated when the reservoir contains numerous aligned structures such as microcracks, fractures, joints, and faults. In the presence of the aligned structures, anisotropy in permeability usually occurs because fluid flow takes place preferentially in the direction of alignment. The purpose of this study is to investigate the effects of these heterogeneous and aligned structures on the transport properties of the porous media containing these structures.

Because of the importance of heterogeneity of permeability distribution, considerable

effort has been placed on the numerical modeling. Brown (1987, 1989) has modeled the transport properties of rock joints with surface roughness, in which he assumed that the local permeability of the joint is controlled by the aperture of the local distance between the two rough surfaces. Because the aperture varies with the roughness throughout the joint, the distribution of permeability is heterogeneous over the joint. Recently, by applying the method of cellular-automata to modeling fluid flow in arbitrarily heterogeneous porous media, Rothman (1988) has successfully modeled the fluid flow in porous media and confirmed the validity of Darcy's law for the heterogeneous media. In most reservoirs the fractures contribute significantly to the permeability and flow of water or oil and gas. Long and Witherspoon (1985) modeled the flow system in terms of fracture network and discussed the effects of connectivity on permeability. In the cases of aligned fractures, the permeability will depend on the direction of alignment, resulting in anisotropy of fluid flow. Gibson and Toksöz (1990) showed that, when the fractures are preferentially aligned in one particular direction (this would result from the preferential closure of cracks subjected to a uniaxial stress), the permeability of such an aligned fracture system varies as a function of the orientation with respect to the alignment. One of the major goals of this study is to numerically test whether or not such alignment of flow channels would result in significant permeability anisotropy and how this anisotropy varies with fracture orientation and connectivity.

In this study, we will apply a finite difference technique to model the flow in porous media. This technique can handle heterogeneities quite easily. We then describe the technique that can generate heterogeneities which can have preferential alignment. We will model fluid flow in various heterogeneous and aligned structures and measure the degree of anisotropy.

THEORETICAL FORMULATION AND NUMERICAL IMPLEMENTATION

In nearly all applications, fluid flow in porous media is assumed to be laminar and is governed by the Darcy's law (Bear, 1972).

$$\vec{q} = -\frac{k}{\mu} \nabla P \ , \tag{1}$$

where $\vec{q}$ is the volume flow rate through unit area, k is permeability, μ is fluid viscosity, and ∇P is pressure gradient. The flow is governed by equation of continuity,

$$\frac{\partial}{\partial t}(\rho\phi) + \nabla \cdot (\rho\vec{q}) = 0 \ , \tag{2}$$

where ϕ is the porosity of the medium, and ρ is the fluid density.

Let $\rho = \rho_0(1 + \frac{P}{\kappa_f})$, where P is fluid pressure and κ_f is the fluid compressibility. Substituting Eq. (1) into Eq. (2) and assuming that $P/\kappa_f \ll 1$, we have

$$\frac{\partial P}{\partial t} = \nabla \cdot (\alpha \nabla P) \ , \tag{3}$$

where $\alpha = \frac{\kappa_f k}{\phi \mu}$ is the pore fluid diffusivity that can vary spatially when the permeability k is heterogeneous. In most reservoir applications, we deal with a pressure field that is steady over time, i.e., $\frac{\partial P}{\partial t} = 0$. In this case, Eq. (3) becomes

$$\nabla \cdot (\alpha \nabla P) = 0 \ . \tag{4}$$

In this study, we are concerned with the two dimensional (2-D) case, i.e., $\frac{\partial}{\partial z} = 0$. Thus, Eq. (4) can be written as

$$\frac{\partial}{\partial x}\left[\alpha(x,y)\frac{\partial P}{\partial x}\right] + \frac{\partial}{\partial y}\left[\alpha(x,y)\frac{\partial P}{\partial y}\right] = 0 \ . \tag{5}$$

Accordingly, Darcy's law in the 2-D case is

$$\begin{cases} q_x = -\frac{k}{\mu}\frac{\partial P}{\partial x} \\ q_y = -\frac{k}{\mu}\frac{\partial P}{\partial y} \end{cases} . \tag{6}$$

Using these equations, we study the fluid flow through a 2-D rectangular grid of length x_0 and width y_0. Fluid pressure is held constant along two opposite sides ($x = 0$ and $x = x_0$). A pressure gradient is set up across the area by setting the pressure on each side to different values. We assume that the other two sides are sealed so that the pressure gradient perpendicular to these sides is set to zero.

Finite Difference Implementation

We use the finite difference technique to solve Eq. (5). Discretizing the rectangular domain $x_0 \times y_0$ into $M \times N$ grids, we have

$$\begin{cases} x = m\Delta x & m = 0, 1, 2, \cdots, M-1 \\ y = n\Delta y & n = 0, 1, 2, \cdots, N-1 \end{cases} \tag{7}$$

and

$$\alpha_{m,n} = \alpha(m\Delta x, n\Delta y) \ . \tag{8}$$

Using the forward difference, Eq. (5) can be written as

$$P_{m,n} = \frac{1}{A_1 + A_2 + d(A_3 + A_4)} [A_1 P_{m+1,n} + A_2 P_{m-1,n} + dA_3 P_{m,n+1} + dA_4 P_{m,n-1}] \tag{9}$$

where

$$\begin{cases} A_1 = \alpha_{m+1,n} + \alpha_{m,n} \\ A_2 = \alpha_{m,n} + \alpha_{m-1,n} \\ A_3 = \alpha_{m,n+1} + \alpha_{m,n} \\ A_4 = \alpha_{m,n} + \alpha_{m,n-1} \end{cases} \tag{10}$$

and $d = \frac{\Delta x^2}{\Delta y^2}$. This results in M×N simultaneous equations. Because M and N can be large, direct solutions using the matrix inversion technique are costly and iteration methods are often used for the solution of Eq. (9). A simple iterative procedure can be constructed based on Eq. (9):

$$P^{k+1}_{m,n} = \frac{1}{A_1 + A_2 + d(A_3 + A_4)} \left[A_1 P^k_{m+1,n} + A_2 P^k_{m-1,n} + dA_3 P^k_{m,n+1} + dA_4 P^k_{m,n-1}\right] . \tag{11}$$

The grids for this iteration scheme are shown in Figure 1a. The iteration begins by assigning an arbitrary pressure distribution over the area. Eq. (11) is then used to iterate until convergence is achieved. In the iteration for the boundary points, boundary conditions are always used.

The Gauss-Seidel method (Ferziger, 1981) can be used to accelerate the iteration. This consists of changing Eq. (11) into

$$P^{k+1}_{m,n} = \frac{1}{A_1 + A_2 + d(A_3 + A_4)} \left[A_1 P^k_{m+1,n} + A_2 P^{k+1}_{m-1,n} + dA_3 P^k_{m,n+1} + dA_4 P^{k+1}_{m,n-1}\right] . \tag{12}$$

The grids for this iteration are shown in Figure 1b. Compared with Figure 1a, this iteration makes use of the results of two neighboring points obtained from the current step (if the iteration starts from left to right and from bottom to top). Because the results of the current step are generally closer to the true results than the results of the previous step, the Gaussian-Seidel iteration converges faster than the simple iteration (Eq. 11). The convergence can further be accelerated by using the successive over-relaxation (SOR) technique (Ferziger, 1981), as given by the following formula:

$$P^{k+1}_{m,n} = \omega Q(m,n,k) + (1-\omega) P^k_{m,n} \ , \tag{13}$$

where $Q(m,n,k)$ is an expression given by Eq. (12), and ω is the optimum relaxation constant given by

$$\omega_{opt} = \frac{2}{1 + \sqrt{1 - |\lambda|^2}} \ , \tag{14}$$

where

$$\lambda = \frac{1}{2}\left(\cos\frac{\pi}{M} + \cos\frac{\pi}{N}\right) \quad . \tag{15}$$

The SOR technique is much more faster than the simple iteration (Eq.11) (Ferziger, 1981). Using the algorithm of iterative procedure, the finite difference system (Eq. 9) can be solved fast and efficiently.

GENERATION OF HETEROGENEOUS AND ANISOTROPIC POROUS MEDIA

In this section, we describe the technique for generating the heterogeneous and anisotropic function $\alpha(x, y)$ for the porous media. Because

$$\alpha = \frac{k(x,y)}{\phi(x,y)}\frac{\kappa_f}{\mu} \quad , \tag{16}$$

we see that a heterogeneous $\alpha(x, y)$ can result from the heterogeneity of both k and ϕ. However, since k and ϕ are closely related (Scheidegger, 1974) the heterogeneities of k and ϕ have the same origin, and the heterogeneity of k can be characterized by that of α.

The stochastic model used in this study is a stationary Gaussian random field with mean $\overline{\varepsilon}$ and standard deviation σ. The spatial auto-correlation function of the random field is

$$C_{\varepsilon\varepsilon}(\vec{x}) = < \varepsilon(\vec{x_1})\varepsilon(\vec{x_1} + \vec{x}) > \tag{17}$$

where $< -- >$ is the expected value and $\vec{x}$ is the lag vector or spatial offset. The power spectrum of the Gaussian field $\varepsilon(x, y)$ is the Fourier transform of the correlation function (Bracewell, 1978), and its phase spectrum is a random process uniformly distributed between 0 and 2π (Priestly, 1981). In this study, we use two correlation functions

$$C_{\varepsilon\varepsilon}(\vec{x}) = e^{-\hat{r}^2} \tag{18}$$

$$C_{\varepsilon\varepsilon}(\vec{x}) = K_0(\hat{r}) \quad , \tag{19}$$

where $e^{-\hat{r}^2}$ is a Gaussian function and $K_0(\hat{r})$, the zero order modified Bessel function, represents the zero order von-Karman correlation function (Frankel and Clayton, 1986, Charrett, 1991), $\hat{r}$ is a dimensionless norm. In the case of isotropic distribution, $\hat{r}$ is

$$\hat{r} = \frac{r}{a} = \frac{\sqrt{x^2 + y^2}}{a} \quad , \tag{20}$$

where a is the correlation length of the heterogeneities. As shown in Frankel and Clayton (1986), the wave number spectrum of the Gaussian function decays rapidly with

wavenumber. Thus the Gaussian heterogeneity lacks high frequency components, and the heterogeneities are smooth. The spectrum of von-Karman function decays with wavenumber k_r as k_r^{-2} (or $k^{-\frac{7-2D}{2}}$, where D is fractal dimension, Brown, 1987), giving a fractal dimension of $D = 2.5$. This represents a self-similar distribution for the heterogeneities (Frankel and Clayton, 1986). The case of anisotropy can be modeled by introducing two different correlation lengths a_1 and a_2. The azimuthal variation can be expressed in terms of the ellipsoidal norm

$$\hat{r}(\vec{x}) = \sqrt{\frac{(x\cos\theta + y\sin\theta)^2}{a_1^2} + \frac{(y\cos\theta - x\sin\theta)^2}{a_2^2}} \tag{21}$$

where θ is the angle between the vector $\vec{x}$ and the x axis. With the use of this dimensionless norm, Eq. (18) or (19) defines an elliptically-shaped 2-D correlation function, whose semi-major axis is aligned in θ direction, and the semi-axes are a_1 and a_2, respectively, yielding an aspect ratio a_1/a_2 for the lineation of the heterogeneities. Figure 2 shows the examples of the isotropic (a) and lineated (anisotropic) (b) correlation functions calculated using the Gaussian function (Eq. 18). In the anisotropic case, $\theta = 45°$, $a_1 = 5a_2$. The 2-D heterogeneities are generated by filtering a 2-D random distribution in which the 2-D correlation function of a given type (Gaussian or fractal) and given parameters (a_1,a_2, and θ) is used as the 2-D filter. The examples of the generated heterogeneities will be given in the next section together with the numerical flow simulation examples.

NUMERICAL RESULTS

The major purpose of these simulations is to study the effects of heterogeneities on the flow through porous media. The flow simulations are done as follows. In the first, the distribution of the fluid diffusivity $\alpha(x, y)$ is generated over the rectangular area $0 < x < x_0$, $0 < y < y_0$. For the given $\alpha(x, y)$ and the boundary conditions, the pressure field $P(x, y)$ is computed by solving the finite difference equation (Eq. 9) using the SOR iterative procedure.

The pressure field is differentiated and used in the Darcy's law to calculate the local volume flow rate vectors, whose components are the terms given in Eq. (6). Plots of these vectors represent the flow field in the 2-D porous medium. The total flow across the $x = x_0$ boundary is given by

$$Q_x = \int_0^{y_0} q_x(x_0, y)dy \ . \tag{22}$$

The total flow is divided by y_0 to give the flow per unit length

$$\overline{q}_x = Q_x/y_0 \ . \tag{23}$$

The effective permeability $\overline{k}$ of the 2-D medium can be measured using the Darcy's law (Eq. 6)

$$\overline{q}_x = -\frac{\overline{k}\,\Delta P}{\mu\ x_0} \ . \tag{24}$$

where ΔP is the difference between the pressures at the two ends of the 2-D model, and $\Delta P/x_0$ represents the macroscopic pressure gradient across the model length x_0 parallel to the no-flow boundaries. In all cases of this study, we assume that the pore fluid is water with $\mu = 1.14 \times 10^{-3}$(Pa s) and $\kappa_f = 2.25$GPa.

Isotropic Distribution

We first study the effects of different heterogeneities on the flow and the effective permeability $\overline{k}$ of the medium. Figure 3 plots two distributions of $\alpha(x, y)$; one is Gaussian (Figure 3a), the other is self-similar (Figure 3c). The distributions are isotropic and have the same correlation lengths $a = 3$. The model lengths are $x_0 = y_0 = 128$.

The fractal distribution (self-similar) is much rougher than the Gaussian distribution. The simulated flow for the two cases is shown in Figures 3b and d. Although the two heterogeneous distributions modify the flow, the difference between the two flow fields is minimal. Figure 4 shows the average flow versus pressure gradient calculated using Eq. (24) for a number of ΔP values. The slope of the line gives the average permeability $\overline{k}$. It can be seen that Darcy's law still holds despite the heterogeneities and that the average permeabilities for the two distributions are very close, although the fractal result shows slightly higher $\overline{k}$ values. This result shows that the total flow is not very sensitive to the details of the heterogeneous distribution (i.e., roughness of the fractal distribution). This agrees with the result obtained by Brown (1987), who showed that the total flow through a joint does not vary significantly with the fractal dimension used to characterize the joint roughness. However, this conclusion is valid only when the correlation length is small compared with the model length. When the ratio of the two lengths a/x_0 increases, the difference between the $\overline{k}$ values of the two distributions will increase. Figures 5a and b show the flow versus pressure gradient for two successively larger a/x_0 ratios, $a/x_0 = 0.047$ (Figure 5a), and $a/x_0 = 0.078$ (Figure 5b) ($a/x_0 = 0.023$ in Figure 4). The permeability difference for the two cases at $\Delta P = 100Pa$ is about 4% and 9%, respectively (it is only 1% in Figure 4).

Aligned Distribution

Using the ellipsoidal norm given in Eq. (21), we can generate aligned distribution for the heterogeneities. In an example shown in Figures 6a, c, and e, we use the same parameters ($\bar{\varepsilon}, \sigma, x_0, y_0$, etc.) as those in the previous isotropic case. The correlation

lengths in the semi-major axial and semi-minor axial directions are $a_1 = 20$ and $a_2 = 2$, respectively. The correlation function is Gaussian (Eq. 18). For $\theta = 0°$, $\theta = 45°$, and $\theta = 90°$, we have calculated the flow fields as shown in Figures 6b, d, and f. Because of the contrast in permeability, the flow tends to channel through high permeability regions. This is clearly shown in the $\theta = 45°$ case, where the lineation of high and low permeability strips makes the flow field have a trend to deflect towards the lineation of the high permeability region. Figure 7 shows the calculated average flow versus θ. The permeability is the maximum along $\theta = 0°$, and becomes minimum along $\theta = 90°$; the anisotropy for this case is about 10%. For comparison, the case of isotropic Gaussian ($a = 20$) is also shown (solid line). By varying the correlation lengths a_1 and a_2, the degree of anisotropy cannot significantly exceed this value. This is due to the random medium model used here. In this model, a region with moderate and low permeabilities is sandwiched between two adjacent high permeability regions. Therefore, flow can always cross the less permeable region without having to flow around the region. Thus, due to the presence of background permeability (small as it is), the lineation of random heterogeneities cannot result in anisotropic permeabilities that are an order of magnitude different. In order to produce such a strong permeability anisotropy, the background permeability must be removed. This will be the case of fractures studied in the following section.

Aligned Fracture Model

Since fractures could contribute significantly to the reservoir permeability, it is important to model the effects of fracture permeability. As shown by Gibson and Toksöz (1990), a primary effect of fracture is anisotropy in permeability. Because of the alignment of fractures, the permeability can vary with orientation by orders of magnitude. The primary interest of this section is to model the effects of fractures on the flow fields. The major features of fracture fluid flow are that the background has negligible permeability, and that the flow is highly concentrated along the fractures. This situation can be modeled using the random medium model as follows. We choose the aspect ratio $a_1/a_2 \gg 1$, so that the heterogeneities are highly lineated. In order to remove the background permeability, we set a threshold, say 60% of the maximum $[\alpha(x, y)]$. The values of $\alpha(x, y)$ that are smaller than this threshold are set to a very small number (this number cannot be set to zero in order to avoid division by zero errors, see Eq. 12), and values greater than the threshold are kept unchanged. Figures 8a, c, and e show the $\alpha(x, y)$ distributions that resemble a natural fracture network. The permeability contrast between the fracture and the background is 600:1. Although the background permeability may still be large compared to typical fractured rocks (granite, limestone, etc.), the highly conductive channels (fractures) conduct most of the flow so that the background flow is small. In this way, the flow in the fracture network is simulated. The calculated flow field along and perpendicular to the fracture alignment is shown in

Figures 8b, d, and f. The flow patterns for the three orientations are quite different. As expected, the flow is highly channeled along fractures. The connectivity of the fractures plays a very important role controlling the flow field. As shown in these figures, fractures that are not connected with the flow source (the $x = 0$ and $x = x_0$ boundaries) have very little flow, while fractures connected with the boundaries conduct most of the flow. For the $\theta = 90°$ case (Figure 8f), the flow has to wind around the junctions of the fractures. While in the $\theta = 0°$ case, flow takes place along the straight channel. This results in significant permeability difference for the two cases. We have performed the calculation for various orientations. The calculated average flow as a function of the orientation θ is shown in Figure 9. In this figure, the permeability is maximum along fractures and minimum perpendicular to them, the same as in the previous case of aligned heterogeneities. However, the permeability difference between $\theta = 0°$ and $\theta = 90°$ is 184% in the previous case. This numerical modeling result confirms the prediction of Gibson and Toksöz (1990) that aligned fractures can have very significant anisotropy.

In the above example, the correlation length a_1 in the lineation direction is comparable to the model length, as in the case assumed by Gibson and Toksöz (1990). In the field, fractures between two wells have limited extent, and the fractures may not be well connected. Long and Witherspoon (1985) pointed out the importance of connectivity on permeability. Here we model how the anisotropy of permeability changes when the connectivity decreases. We first generate the lineated heterogeneities with $a_1 = 5$, $a_2 = 1$; the model length is 128. The lineated fractures are shown in Figure 9. Compared with the fracture system shown in Figure 8, fractures in this case have a much lower degree of connectivity. Figures 10b, d, and f show the flow fields for $\theta = 0°$, $\theta = 45°$, and $\theta = 90°$ cases. For $\theta = 0°$, the average permeability is only 25 mD, much decreased from the well connected case of Figure 9, in which the average permeability at $\theta = 0°$ is about 2.5D. Because of the decreased connectivity due to shorter fracture lengths, flow can take a "shorter cut" winding around fractures in the $\theta = 90°$ case. As a result, anisotropy is not as significant as the well connected case of Figure 9. Figure 11 shows the calculated average flow versus θ. The anisotropy is still present, but the difference between $\theta = 0°$ and $\theta = 90°$ is now about 87%, much lower than the previous case of 184% (Figure 9). This example demonstrates that not only the fracture orientation, but also the connectivity of fractures are important in controlling the anisotropy of fracture permeability.

CONCLUSIONS

In this study, we have developed an effective finite difference algorithm for modeling fluid flow in arbitrarily heterogeneous porous media. We have shown that Darcy's law is valid for any heterogeneous and anisotropic distributions of permeability. The

flow is not sensitive to the roughness of the distribution, but may be affected by the lineation in the permeability distribution. However, due to the presence of background permeability, the lineation of highly permeable regions and less permeable surroundings does not result in anisotropy of an order of magnitude. Nevertheless, in cases of aligned fractures where the background permeability is small, such significant anisotropy does exist for well connected aligned fractures. The anisotropy will be decreased as fracture connectivity decreases.

It is straightforward to generate the finite difference modeling to the fully anisotropic case. We will perform this calculation in the research that follows. It is interesting to compare the anisotropic solution and the solution for the anisotropic permeability distribution. In addition, since some laboratory measurements are the response of the porous media to preesure transients to characterize rock heterogeneities (Kamath et al., 1990), the finite difference code for the diffusion equation (Eq. 3) can be developed to study the effects of heterogeneities and anisotropy on the time-dependent flow properties.

ACKNOWLEDGEMENTS

We would like to thank Yves Bernabe for his fruitful discussions. This research was supported by Department of Energy Grant #DE-FG02-86ER13636 and the Full Waveform Acoustic Logging Consortium at M.I.T.

REFERENCES

Bracewell, R., *The Fourier Transform and its Applications*, McGraw-Hill, New York, 1978.

Brown, S., Flow through rock joints: the effects of surface roughness, *J. Geophys., Res., 92*, 1337–1347, 1987.

Brown, S., Transport of fluid and electric current through a single fracture, *J. Geophys., Res., 94*, 9429–9438, 1989.

Bear, L., *Dynamics of Fluids in Porous Media*, Elsevier, New York, 1972.

Charrett, E.E., *Elastic Wave Scattering in Laterally Inhomogeneous Media,* Ph.D. Thesis, Massachusetts Institute of Technology, Cambridge, Massachusetts, 1991.

Ferziger, J.H., *Numerical Methods for Engineering Applications*, John Wiley & Sons, Inc., New York, 1981.

Frankel, A., and R. Clayton, Finite difference simulations of seismic scattering: implications for the propagation of short-period seismic waves in the crust and models of crustal heterogeneity, *J. Geophys. Res., 91*, 6465–6489, 1986.

Gibson, R.L., Jr., and M.N. Toksöz, Permeability estimation from velocity anisotropy in fractured rock, *J. Geophys. Res., 95*, 15643–15655, 1990.

Kamath, J., R.E. Boyer, and F.M. Nakagawa, Characterization of core scale heterogeneities using laboratory pressure transients, *Society of Petroleum Engineers*, 475–488, 1990.

Long, C.S., and P.A. Witherspoon, The relationship of the degree of interconnection to permeability in fracture networks, *J. Geophys. Res., 90*, 3087–3098, 1985.

Priestly, M.B., *Spectral Analysis and Time Series*, Academic Press, San Diego, 1981.

Rothman, D.H., Cellular-automaton fluids: A model for flow in porous media, *Geophysics, 53*, 509–518, 1987.

Scheidegger, A.E., *The physics of flow through porous media*, Univ. Toronto Press, Toronto, 1974.

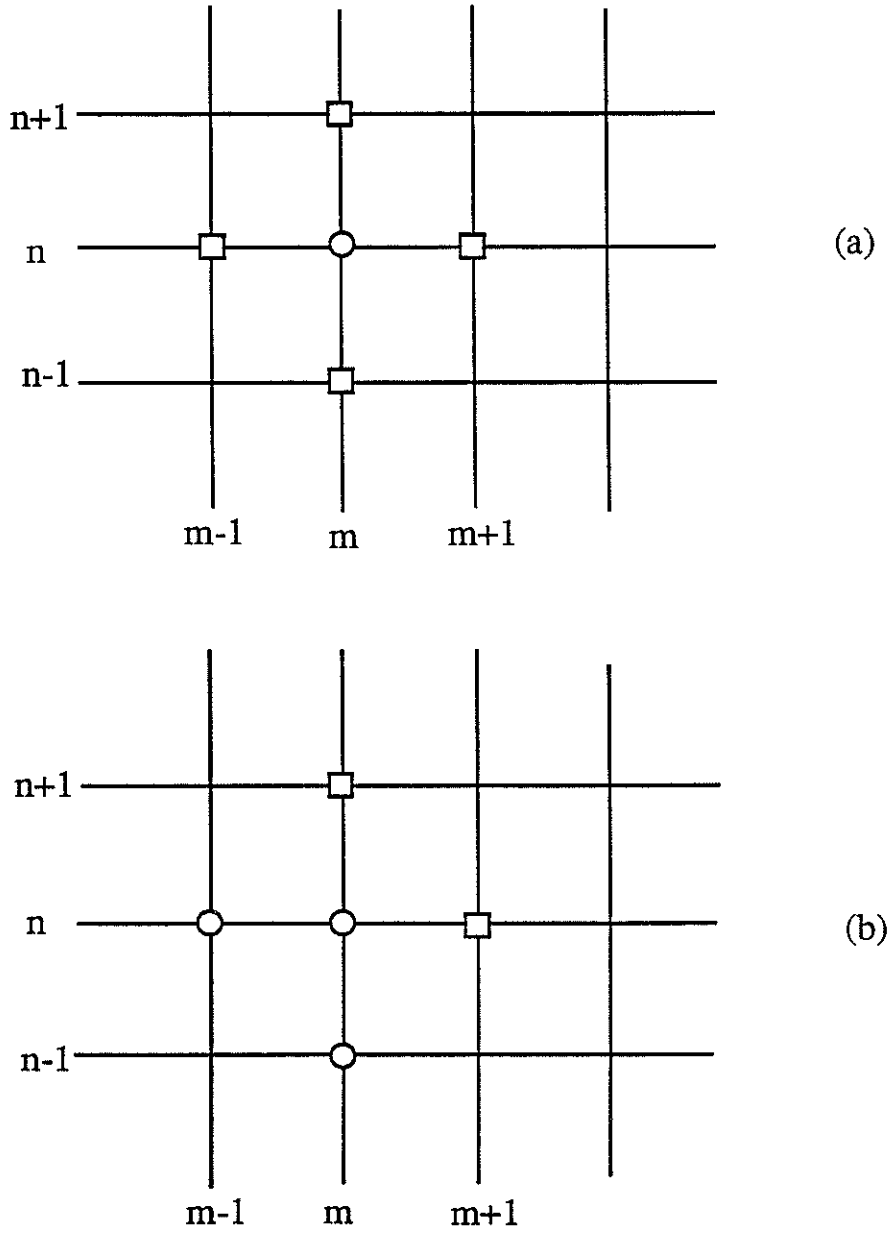

Figure 1: (a). Finite difference grids for the simple iteration. (b). Finite difference grids for Gauss-Seidel iteration. In both (a) and (b), open circles denote current step and open squares denote previous step.

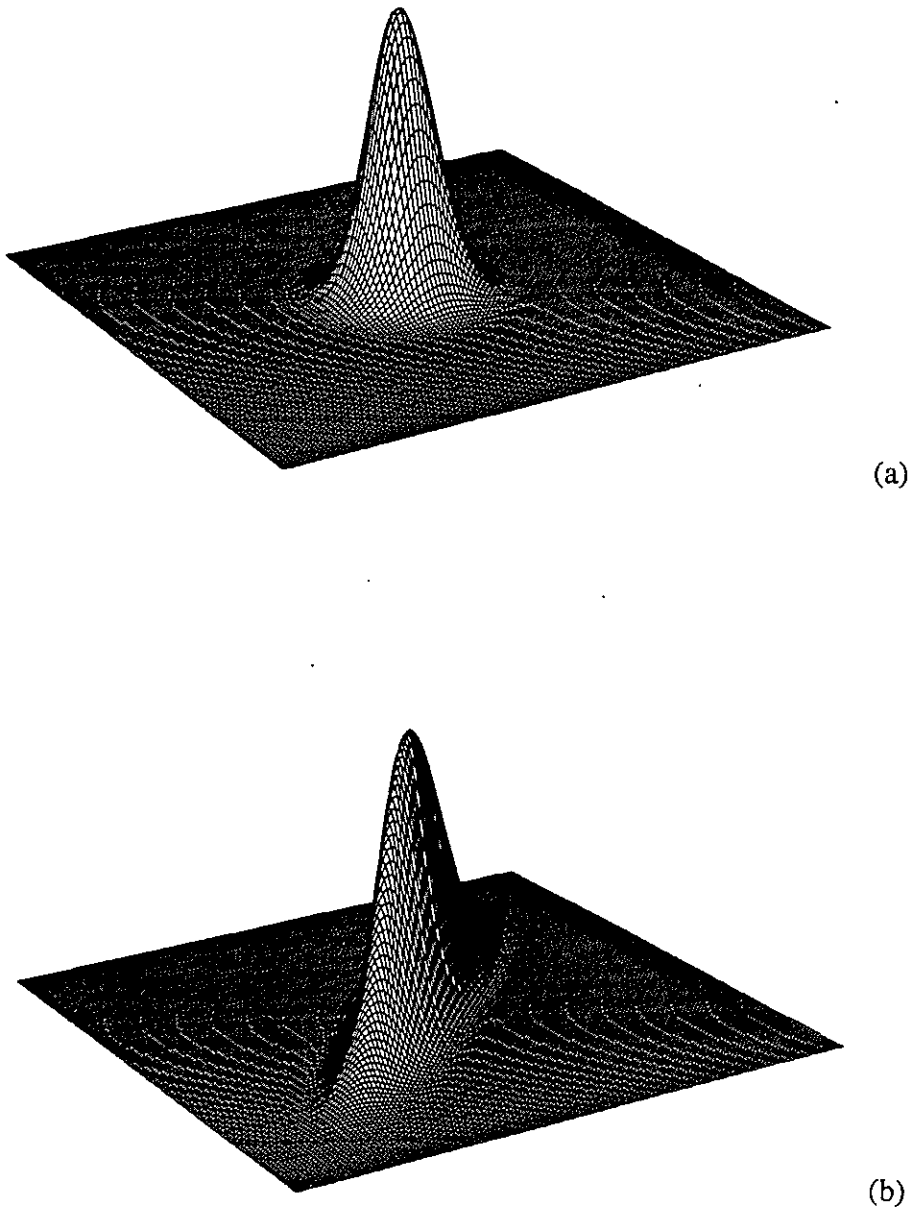

Figure 2: Examples of 2-D correlation function (Gaussian) used to generate heterogeneities. (a) isotropic case (correlation length $a = 10$). (b) anisotropic case (the two correlation lengths are $a_1 = 20$, and $a_2 = 4$. The angle of alignment is $\theta = 45°$).

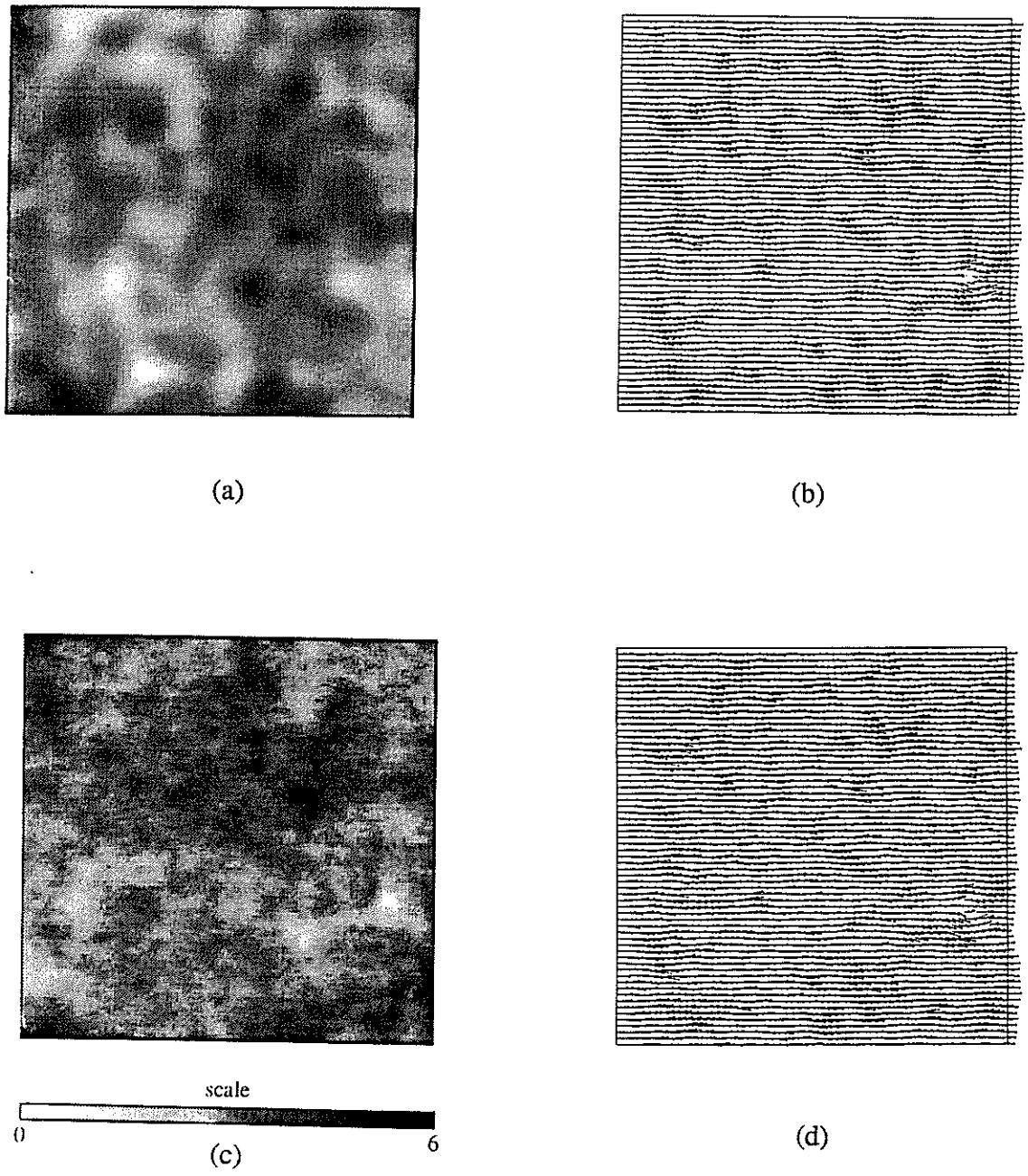

Figure 3: (a) and (c): Isotropic distributions of $\alpha(x, y)$ generated by Gaussian (a) and Fractal (c) correlation functions. In both cases the correlation length is the same. (b) and (d): the simulated flow field for the Gaussian (b) and fractal (d) cases. The flow vectors are normalized by the maximum amplitude.

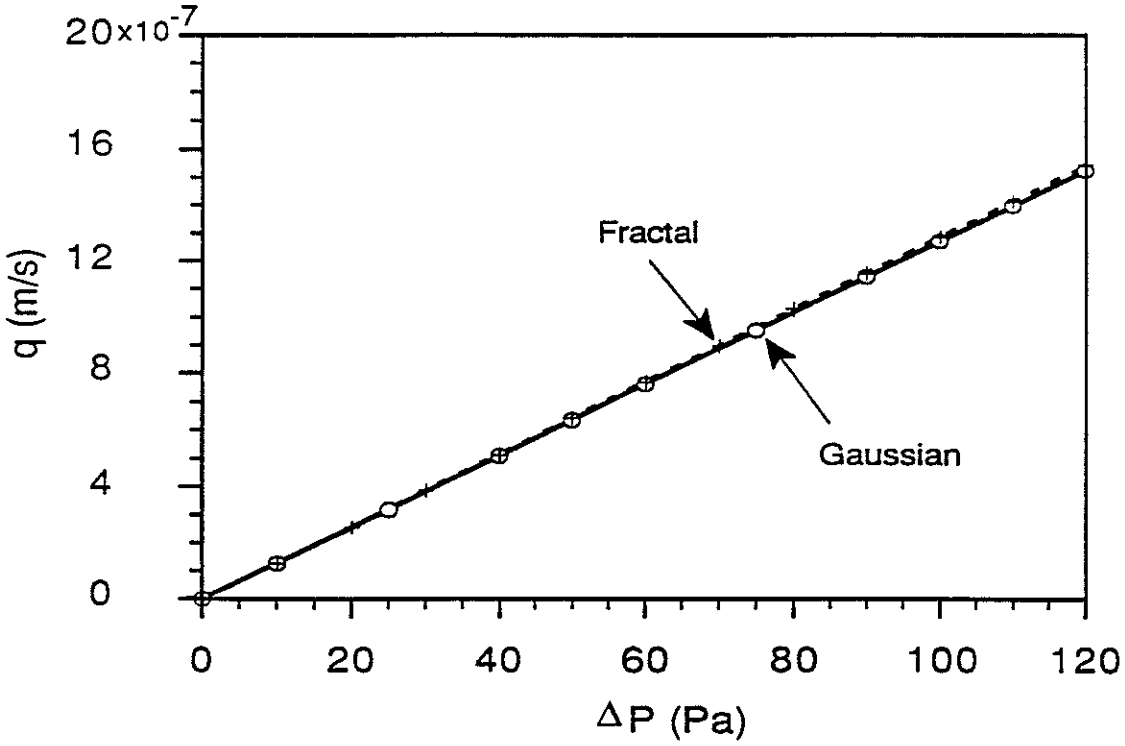

Figure 4: Flow versus pressure gradient for the Gaussian (solid) and fractal (dashed) distributions shown in Figures 3a and 3c. The slope of the lines gives the average permeability $\overline{k}$ of the medium. In the both cases, the $\overline{k}$ values are very close. The permeability difference is only 1%.

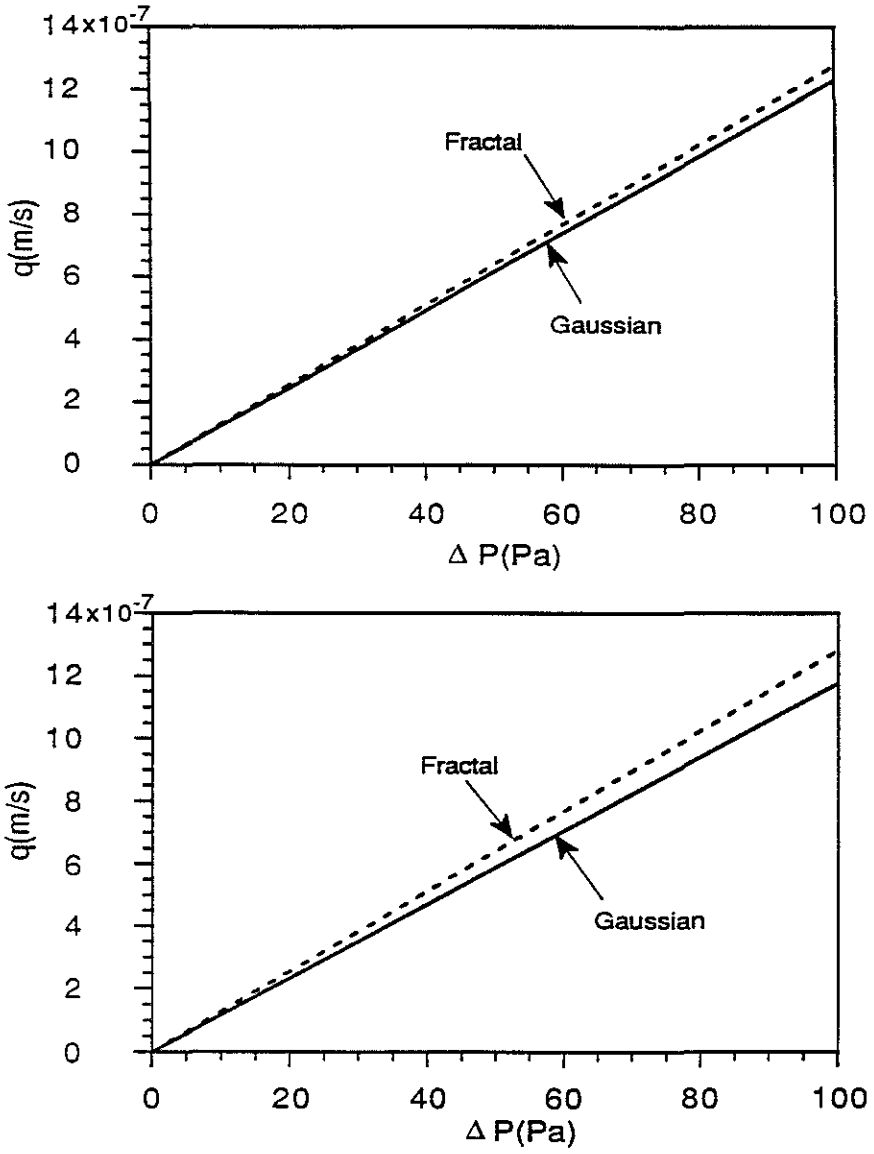

Figure 5: Same as Figure 4, but now the ratio of correlation length to the model length is increases. In (a) the ratio is about 0.047, in (b) it is 0.078. The fractal distribution has a higher $\overline{k}$ value than the Gaussian when correlation length is increased. The differences are about 4% in (a) and 9% in (b).

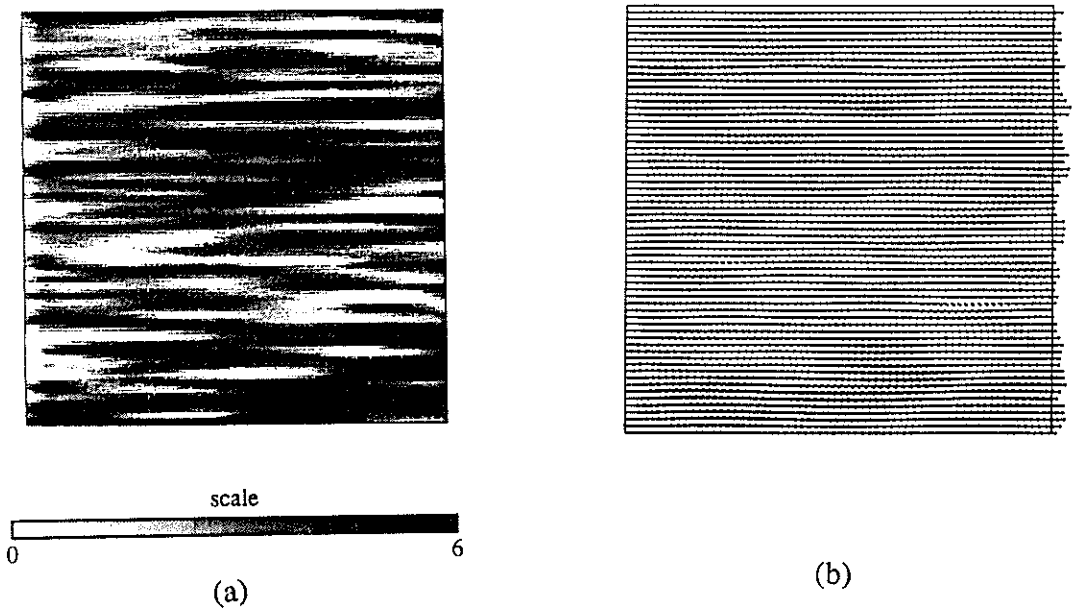

Figure 6: (a), (c), and (e): aligned distributions with $\theta = 0°$ (a), 45° (c), and 90° (e) calculated using Gaussian correlation functions. The two correlation lengths are $a_1 = 20$, $a_2 = 2$. Model lengths are $x_0 = y_0 = 128$. (b), (d), and (f): calculated flow fields for $\theta = 0°$ (b), 45° (d), 90°(f).

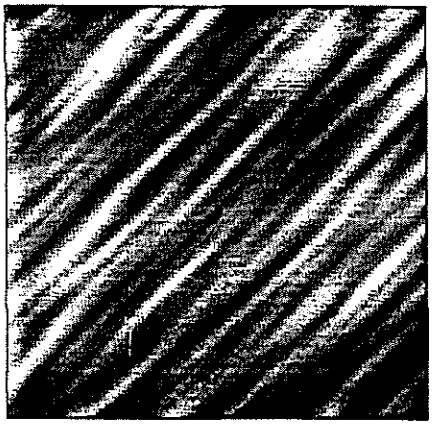

(c)

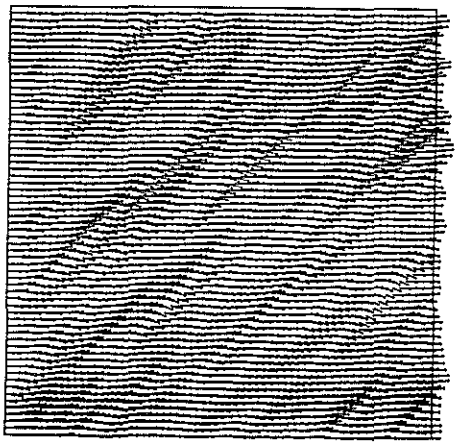

(d)

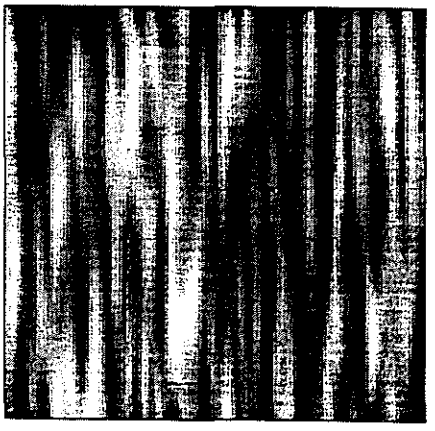

(e)

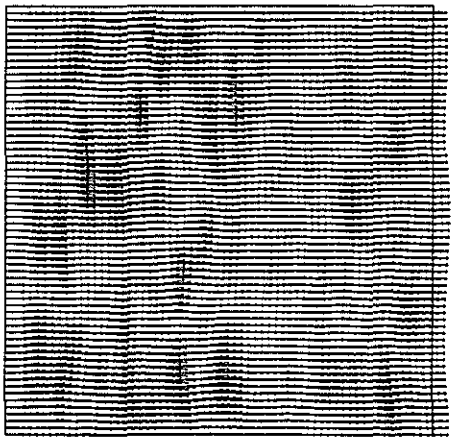

(f)

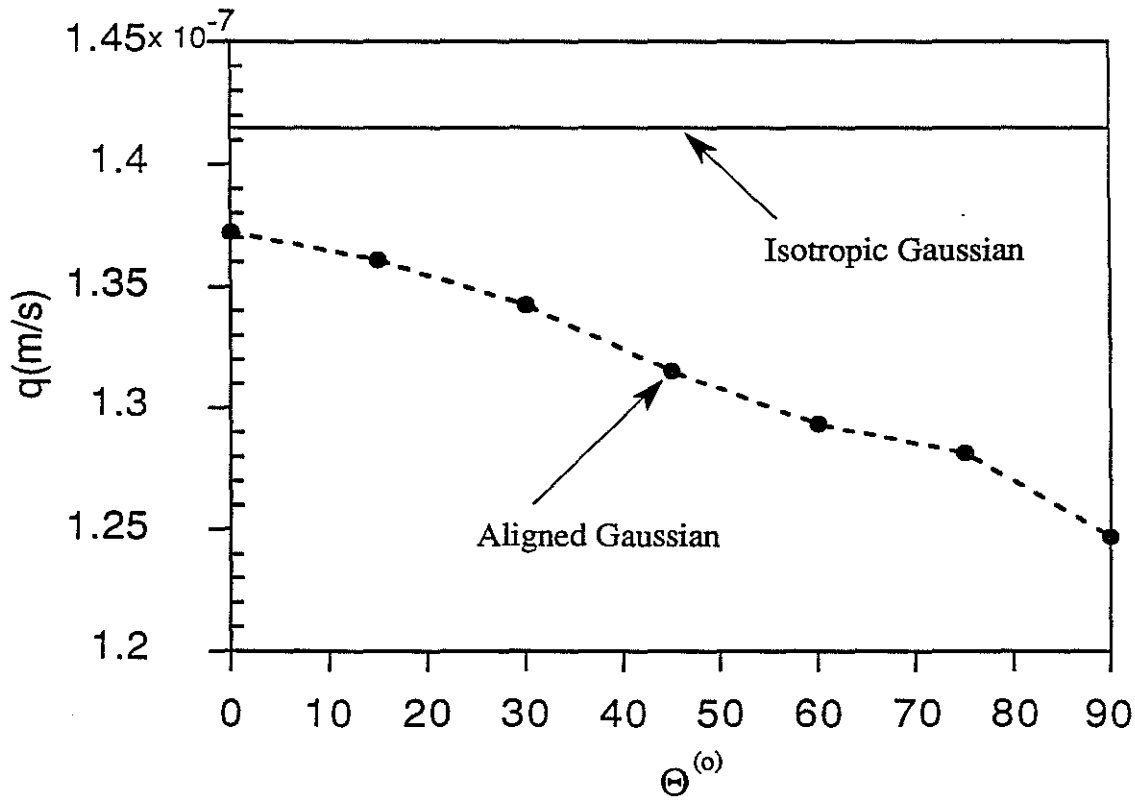

Figure 7: Average flow $\bar{q}$ versus angle of alignment for the cases of Figure 6. The case of isotropic Gaussian ($a = 20$) is also plotted for comparison (solid line). Although permeability anisotropy is present, its magnitude is only about 10%.

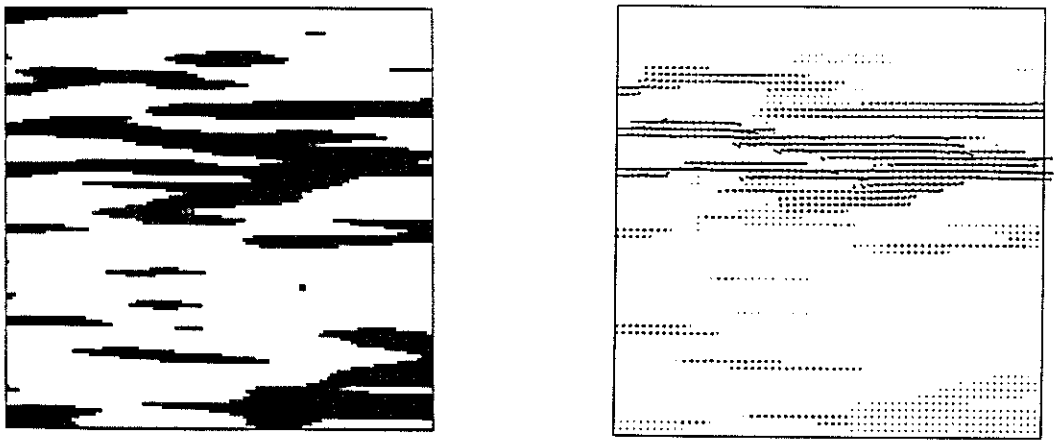

(a) (b)

Figure 8: (a), (c), and (e): aligned fracture permeability distributions with $\theta = 0°$ (a), 45° (c), and 90° (e). The correlation lengths and model lengths are the same as in Figure 6. (b), (d), and (f): calculated flow for $\theta = 0°(b)$, 45° (d), 90° (f).

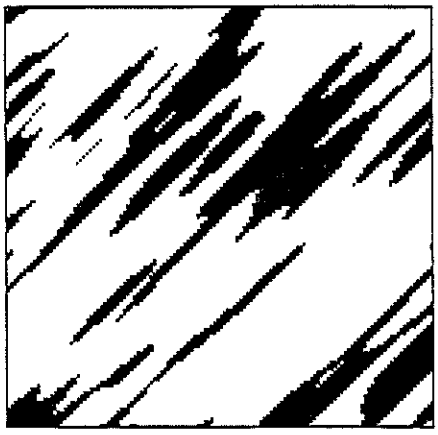

(c)

(d)

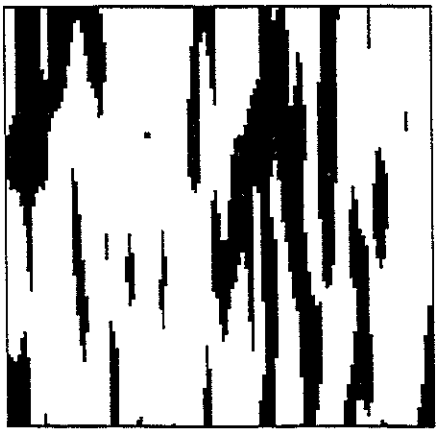

(e)

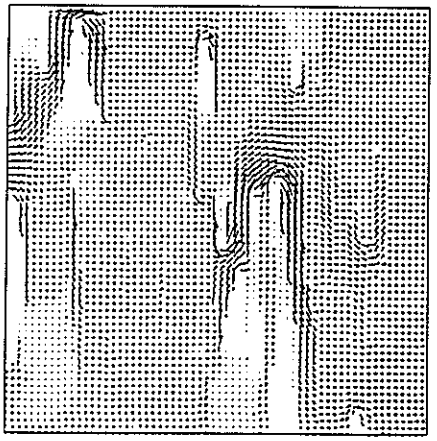

(f)

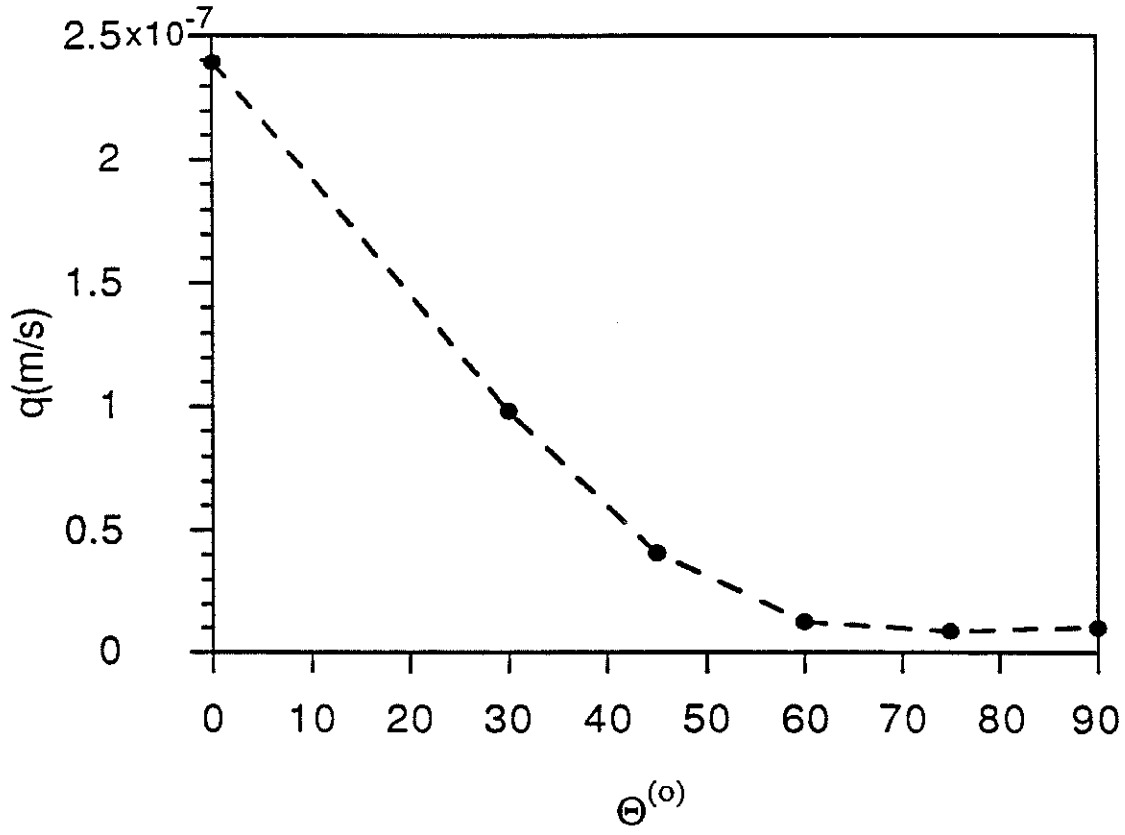

Figure 9: Average flow vs. θ for the case of Figure 8. In the case of aligned fractures, $\overline{k}$ can have order of magnitude difference between $\theta = 0°$ and $\theta = 90°$, resulting in significant anisotropy (about 184%).

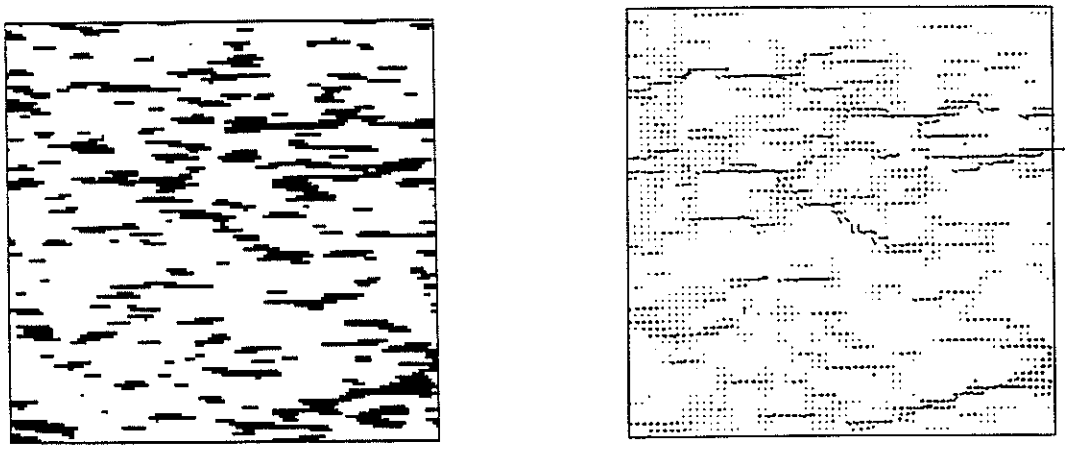

(a) (b)

Figure 10: Same as Figure 8, but now the correlation lengths are reduced to $a_1 = 5$ and $a_2 = 1$. In this way, the connectivity of fractures is reduced.

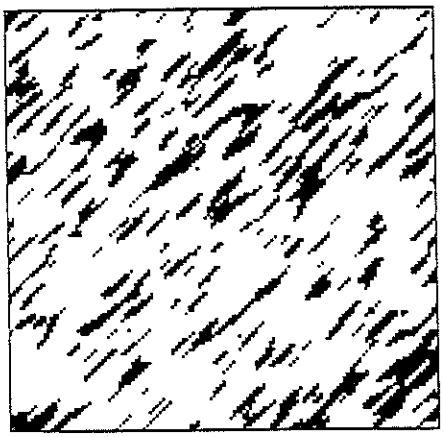

(c)

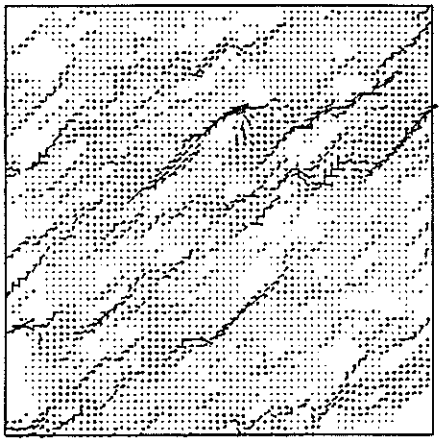

(d)

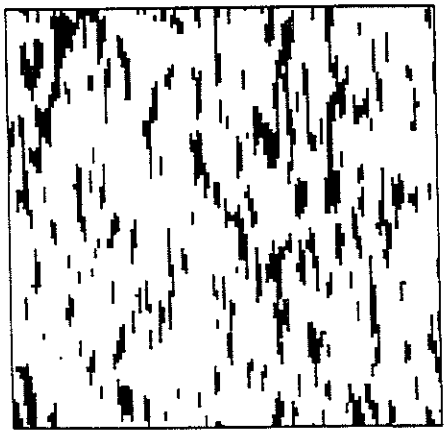

(e)

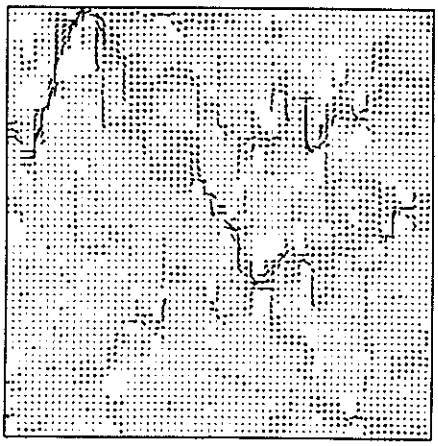

(f)

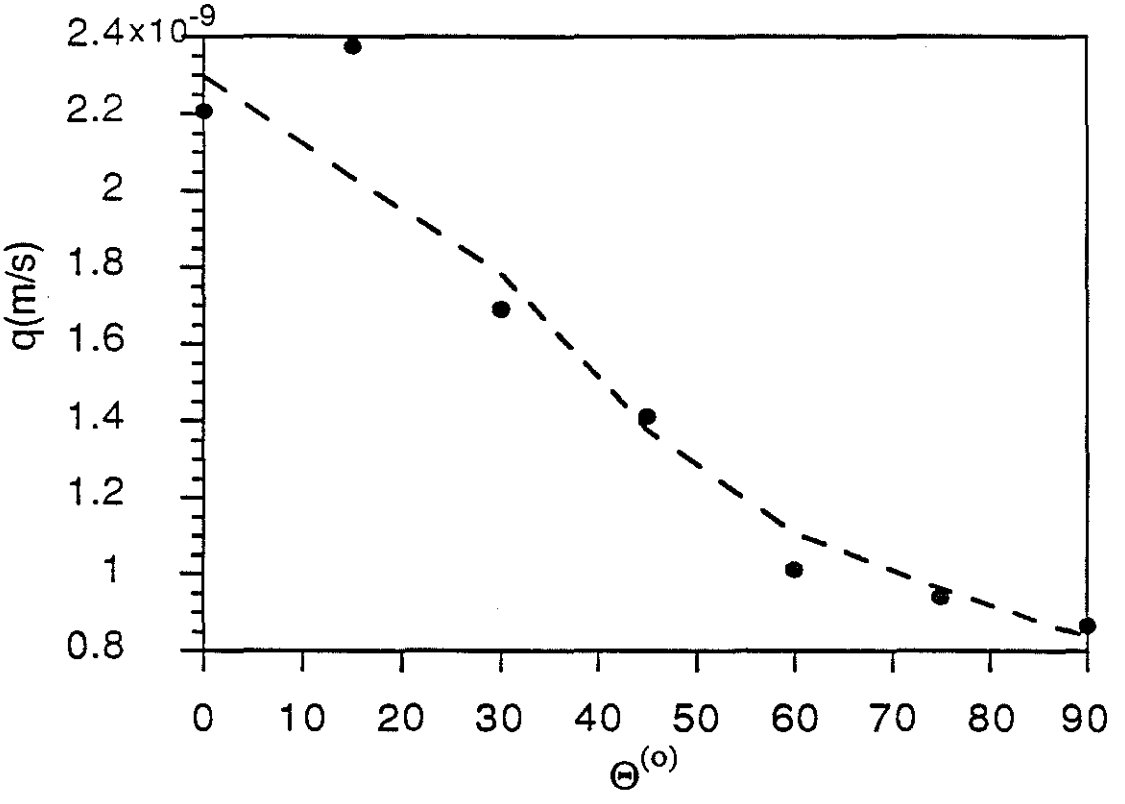

Figure 11: Average flow vs. θ for the case of Figure 10. Compared with Figure 9, the degree of anisotropy is reduced with reduction of the connectivity of fractures. The permeability difference between $\theta = 0°$ and $\theta = 90°$ is about 87%.